Thermochimica Acta 477 (2008) 25–31

Contents lists available at ScienceDirect

Thermochimica Acta

journal homepage: www.elsevier.com/locate/tca

Polymer nanoparticles to decrease thermal conductivity of phase change materials

Fabien Salaün[a,*], Eric Devaux[a], Serge Bourbigot[b], Pascal Rumeau[c], Pierre-Olivier Chapuis[d], Sourabh Kumar Saha[d], Sebastian Volz[d]

[a] *Laboratoire de Génie et Matériaux Textiles (GEMTEX), UPRES EA2461, Ecole Nationale Supérieure des Arts et Industries Textiles (ENSAIT), 9 rue de l'Ermitage, BP 30329, 59056 Roubaix Cedex 01, France*
[b] *Procédés d'Élaboration des Revêtements Fonctionnels (PERF), LSPES UMR-CNRS 8008, École Nationale Supérieure de Chimie de Lille (ENSCL), BP 90108, 59652 Villeneuve d'Ascq Cedex, France*
[c] *Institut Français du Textile et de l'Habillement, Direction Régionale Rhône-Alpes PACA, Avenue Guy de Collongue, 69134 ECULLY Cedex, France*
[d] *Laboratoire d'Energétique Moléculaire et Macroscopique, Combustion, UPR CNRS 288, Ecole Centrale Paris, Grande Voie des Vignes, 92295 Châtenay Malabry, France*

ARTICLE INFO

Article history:
Received 7 May 2008
Received in revised form 21 July 2008
Accepted 23 July 2008
Available online 5 August 2008

Keywords:
Nanocapsules
Phase change microcapsules
Microencapsulation

ABSTRACT

Microcapsules including paraffin are currently used for textiles coating in order to deaden thermal shocks. The microparticles comprising a mixture of paraffin and nanoparticles of poly(vinyl) alcohol/hydrated salt crosslinked by methylene diisocyanate entrapped in melamine-formaldehyde resin shell were prepared through in situ polymerization. The influences of nanoparticles on the thermal properties of microcapsules were investigated using scanning thermal microscopy and differential scanning calorimetry (DSC). It was stated that polymer nanoparticles embedded in those microsized capsules allow to decrease the thermal conductivity of the coating and to enhance the protection in the stationary regime. A reasonable volume fraction of polymer nanoparticles reduces the conductivity more than predicted by Maxwell mixing rules. Besides, measurements prove that the polymer nanoparticles do not affect the latent heat and even improve the phase change behaviour as well as the mechanical properties.

1. Introduction

In the two past decades, microencapsulated Phase Change Materials (PCM) have drawn an increasing interest to provide enhanced thermal functionalities in a wide variety of applications [1–4]. When the encapsulated PCM is heated to above its phase change temperature, it absorbs heat as it goes from a solid state to a liquid state or during a solid-to-solid transition. It can be applied to clothes technology [5], building insulation [6], energy storage as well as to coolant liquids [7]. On a more general basis, it can be used to design a broad variety of thermal transient regimes.

Up to now, most studies have targeted microcapsules [8–14], but encapsulation of micro-nanospheres remains an innovative field [15]. Furthermore, the synthesis of composite polymer microparticles containing an inorganic component has attracted considerable attention to prepare novel functional materials. Thus, the incorporation of inorganic nanoparticles allows to increase thermal stability and mechanical strength of the polymeric microparticles [16].

In the present article, the influence of nanoparticles on the structure and the thermomechanical properties of the microcapsules were studied with differential scanning calorimetry (DSC), scanning thermal microscopy and scanning electron microscopy (SEM). The aim of this work is to compare the microcapsules structural modifications and the thermal properties in relation with the chemical structure and core content of the microcapsules. The phase change behavior was characterized by conventional DSC to measure the latent heat and the temperature range of the solid-liquid transition. The thermal conductivity (W/mK) was measured with a Scanning Thermal Microscope because the conventional methods are difficult to apply. Contact technique such as hot guarded plates introduce thermal contact resistances which are difficult to estimate and the low optical absorption of porous materials makes the application of optical techniques intricate. In this work, we show how polymer nanoparticles (NP) embedded in PCM microcapsules affect the thermal conductivity and can improve the thermal barrier effect. Furthermore, we also focused on the contribution of NP on the phase change behavior and the mechanical properties of the modified microcapsules.

* Corresponding author. Tel.: +333 20 25 64 59; fax: +333 20 27 25 97.
E-mail address: fabien.salaun@ensait.fr (F. Salaün).

0040-6031/$ – see front matter © 2008 Elsevier B.V. All rights reserved.
doi:10.1016/j.tca.2008.07.006

Table 1
Typical composition of inner phase for preparation of microparticles

Samples code	Core composition (wt.%)	Core content in particles	
		n-Alkane (wt.%)[a]	DSP (wt.%)[b]
ARD	*n*-Eicosane/*n*-hexadecane/tetraethyl orthosilicate 48/48/4	75.6	–
18	PVA-MDI/DSP nanoparticles 100	–	16.1
E2	*n*-Eicosane/(PVA-MDI/DSP) 68/32	68.1	3.6
H/E	*n*-Eicosane/*n*-hexadecane /(PVA-MDI/DSP) 34/34/32	72.0	4.4

[a] Determined by DSC.
[b] Calculated from EDAX analysis.

2. Experimental

2.1. Materials

Disodium hydrogen phosphate dodecahydrate, Na_2HPO_4, $12H_2O$ (DSP), *n*-hexadecane, *n*-eicosane and tetraethyl orthosilicate used as PCMs formulation were purchased from Acros organics and used as core material. Poly(vinyl alcohol) (PVA) 95% hydrolysed (M_w = 95,000) from Acros Organics was used to nanoencapsulate DSP. The crosslinking of PVA was carried out using diphenyl methylene diisocyanate (MDI) (Suprasec 2030, Hüntsman ICI) kindly supplied by Hüntsman ICI. Melamine-formaldehyde resin (Arkofix NM) was used as shell-forming materials to prepare microparticles and was kindly supplied by Clariant (France). Arkofix NM is a melamine-formaldehyde precondensate in aqueous solution (68 wt.%). Polyoxyethylene (20) sorbitan monolaurate (i.e. Tween® 20), obtained from Acros Organics, and Polyoxyethylene 23 lauryl ether (i.e. Brij® 35), sorbitan trioleate (i.e. Span® 85), poly(ethylene glycol) dioleate (PEG 400 dioleate) purchased from Aldrich, were used as surfactants. For pH control, triethanolamine and citric acid were used (Aldrich).

2.2. Preparation of various particles

The microencapsulation of various core materials was carried out in a 500 mL three-necked round-bottomed flask equipped with a mechanical stirrer via an in situ polymerization. The preparation conditions and the corresponding adopted nomenclature are summarized in Table 1. Four types of particles were synthesized, e.g. a core-shell microcapsule labeled 'ARD'; a matricial type nanoparticles labeled '18'; and two multinuclear microparticles containing nanoparticles and either *n*-eicosane (labeled 'E2') or a ternary mixture of *n*-hexadecane/*n*-eicosane/tetraethyl orthosilicate (labeled 'H/E')

2.3. Preparation of sample labeled 'ARD'

The microencapsulation of a ternary mixture of *n*-hexadecane, *n*-eicosane and tetraethyl orthosilicate (48/48/4 wt.%) was carried out in a 500 mL three-necked round-bottomed flask equipped with a mechanical stirrer via an in situ polymerization. Prior to the encapsulation, *n*-hexadecane, *n*-eicosane and tetraethyl orthosilicate were emulsified into an aqueous solution of Arkofix NM containing a binary mixture of Tween® 20 and Brij® 35 at pH 4 at 8000 rpm using ultra turrax high speed homogenizer (Ika T 25 basic, Germany). Finally, the reaction mixture was heated at 60 °C, stirring was continued using a blade stirrer at low speed (400 rpm, RW20, IKA, Germany) for 4 h until the end of the polycondensation. Then the pH of the solution was adjusted to 9 with 50 wt.% triethanolamine solution to complete the reaction. The suspension was cooled to 25 °C and filtered, the microcapsules were washed twice with methanol and distilled water. The ability of amino resins for self-condensation around the core material droplet is linked to its surface activity and is an enrichment of resin molecules within the interface. The concentration of reactive resin molecules in the boundary layer is enhanced by hydrophilic/hydrophobic interactions of the partial methylolated melamine. Thus, the resin condensation proceeds much faster in the boundary layer than in the volume phase, allowing the formation of tougher capsule walls.

2.4. Preparation of sample labeled '18'

4 g of DSP and 2 g of water were mixed and added to a solution of 0.5 g of mixture of nonionic surfactants (1/3 of Span® 85 + 2/3 PEG 400 dioleate) in 7 g of *n*-alkane (either *n*-eicosane or a ternary mixture of *n*-hexadecane, *n*-eicosane and tetraethyl orthosilicate (48/48/4 wt.%)) to obtain emulsion 1. After stirring during 15 min, the droplet size was reduced by homogenizing the emulsion during 15 min at 9500 rpm using ultra turrax high speed homogenizer (Ika T 25 basic, Germany). In the same way, another emulsion (emulsion 2) was prepared by homogenizing 8 g of PVA solution (5 wt.%) in 8 g of *n*-alkane. The particles '18' were prepared by shearing under high speed the two emulsions (emulsions 1 and 2) with 3 g of MDI to crosslink the shell at 50 °C for 30 min. The resulting polymer nanoparticles were observed under SEM as illustrated in Fig. 1.

2.5. Preparation of samples labeled 'E2' and 'H/E'

The resultant solution of batch '18' containing the nanoparticles in a paraffinic medium was emulsified in an aqueous solution containing 4 g of Tween® 20 in 100 g of water and 9.2 g of Arkofix NM. The pH was reduced to 3 by adding citric acid solution (30 wt.%), at a stirring rate of 8000 rpm at room temperature with a homogenizer. After 3 min, the reaction mixture was heated at 60 °C, whereas stirring was continued using a blade stirrer at 400 rpm for 4 h until the end of the polycondensation. Finally the microparticles were recovered by filtration, washed with methanol and water, and dried at room temperature during one night.

According to the paraffinic medium used in the preparation of sample '18', either *n*-eicosane or a ternary mixture (*n*-hexadecane, *n*-eicosane and tetraethyl orthosilicate – 48/48/4 wt.%), two types of multinuclear microparticles were obtained 'E2' and 'H/E', respectively.

3. Analytical methods

The thermal behavior of the particles was recorded using a TA instrument type DSC 2920 with TA Advantage control software. Indium was used as standard for temperature calibration and the analysis was made under a constant stream of nitrogen (50 mL min^{-1}). Samples were placed in aluminum pans which were hermetically sealed before being placed on the calorimeter thermocouples. The sample space was purged with nitrogen at a constant flow (50 mL min^{-1}) during the experiments and the temperature range was from −30 to 100 °C. Transition temperatures and enthalpies were obtained by averaging the results of a series

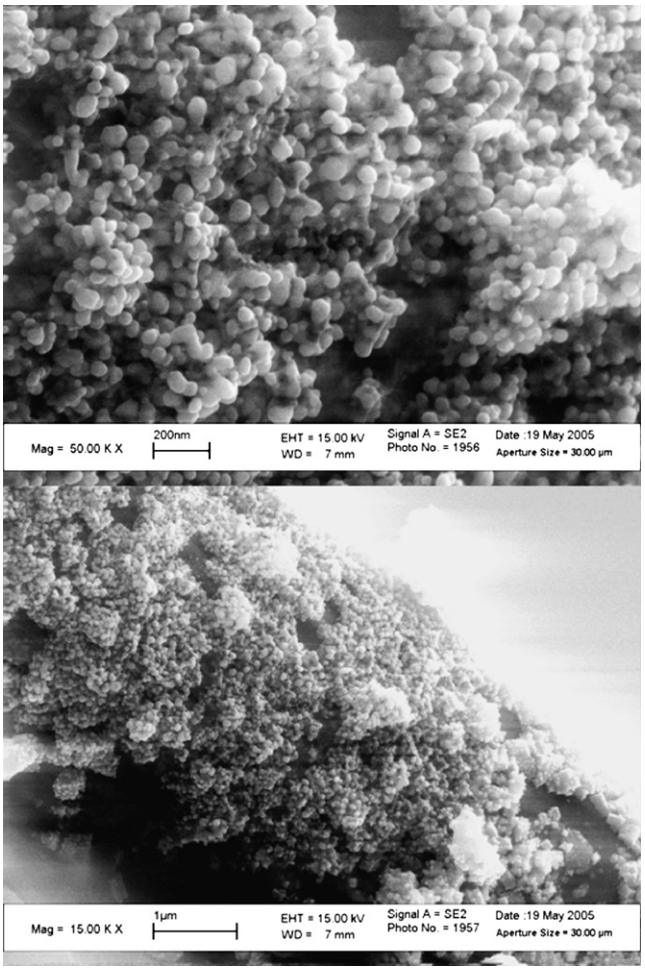

Fig. 1. Scanning Electron Microscope image of sample 18. The polymer nanoparticles have diameters of about 50 nm. The high particle density allows for aggregation.

of four independent experiments on (4.0±) – mg samples with different scanning speeds, e.g. 0.5, 2, 5, 10 and 20 K min^{-1}.

The core content in particles was determined by DSC (for *n*-alkane content) and/or EDAX analysis (for hydrated salt content) and expressed as percentage (Table 1).

The microscopic aspects of the microcapsules were observed with optical microscopy (Axioskos Zeiss) equipped with a camera (IVC 800 12S) and with scanning electron microscopy (Philips XL30 ESEM/EDAX-SAPPHIRE).

The thermal conductivity is estimated by using a scanning thermal microscope. It consists in a conventional atomic force microscope mounted with a hot wire probe as illustrated in Fig. 2. The probe is a wollaston wire made of a platinum core 5 μm in diameter and a silver coating 70 μm in diameter. The silver coating is etched to uncover the platinum wire over a length of $2L = 200$ μm. This tip was studied in several of our previous works [17]. A modulated (AC) electrical current is used to heat the Pt/Rh wire by Joule effect and the second harmonic of the temperature is measured. The third harmonic of the tip voltage is recorded because it is proportional to the tip temperature amplitude according to the well-known 3w technique [18]. The wire temperature is related to the heat flux flowing from the hot tip to the cold sample. And this heat flux relating the tip temperature and the sample temperature far from the surface is driven by a thermal conductance G_{eq}. G_{eq} is the contact conductance between probe and sample and the conductance of the sample Gs in series. The sample conductance G_s is

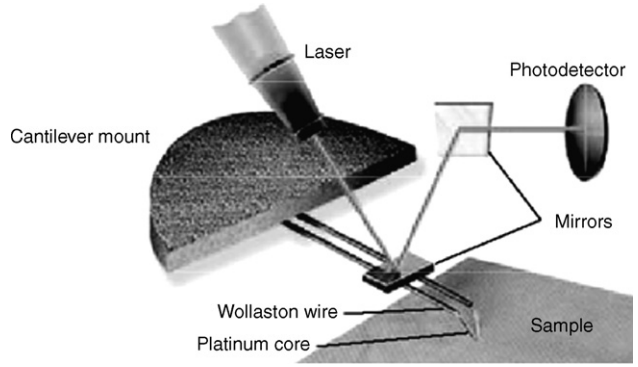

Fig. 2. Sketch of the thermal probe. A wollaston wire is formed as a tip. A mirror is stuck on the top face to allow for the detection of the tip deflection. The electrical resistance of the wire is measured to deduce its temperature and its dissipated heat flux.

the proportionality coefficient between the heat flux from the tip to the sample and the temperature difference between the sample surface under the tip and the sample temperature far from the surface, which can be assimilated to the room temperature. This model is extensively developed in our previous publication [19].

We perform a two-step approach to identify the ratio between two thermal conductivities λ_{S1} and λ_{S2} of two different samples. Measurements are performed in ambient and in vacuum when varying contact force F between sample and tip. Those measurements provide the force derivatives of the sample conductance and the one of G_{eq}. We assume that the contact conductance and the contact hardness do not vary significantly when probing the two dissimilar samples. In those conditions, it can be shown that the ratio between both thermal conductivities arises as follows:

$$\frac{\lambda_{S1}}{\lambda_{S2}} = \left(\frac{dG_S/dF|_1}{dG_S/dF|_2}\right)^{1/2} \left(\frac{dG_{eq}/dF|_2}{dG_{eq}/dF|_1}\right)^{1/4} \quad (1)$$

4. Results and discussion

4.1. Morphologies of microparticles

As shown in Fig. 3, the resulting core-shell microcapsules named 'ARD' have relatively uniform sizes, spherical shape and smooth surface. No destruction of the capsule walls due to mechanical

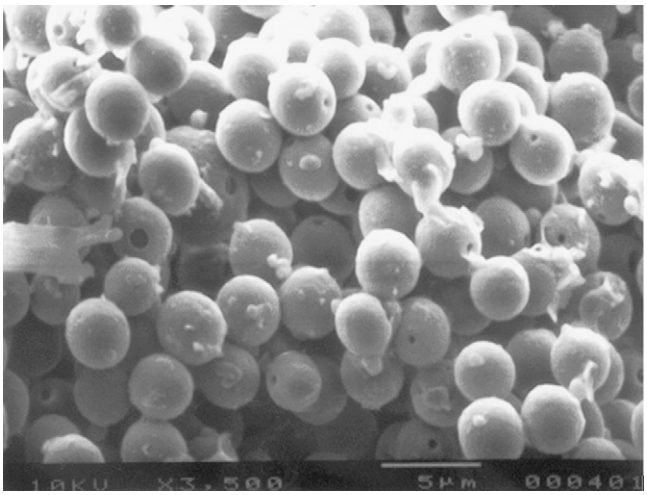

Fig. 3. Scanning Electron Microscope image of the ARD sample. The spherical shell structure has a size of 1–3 μm.

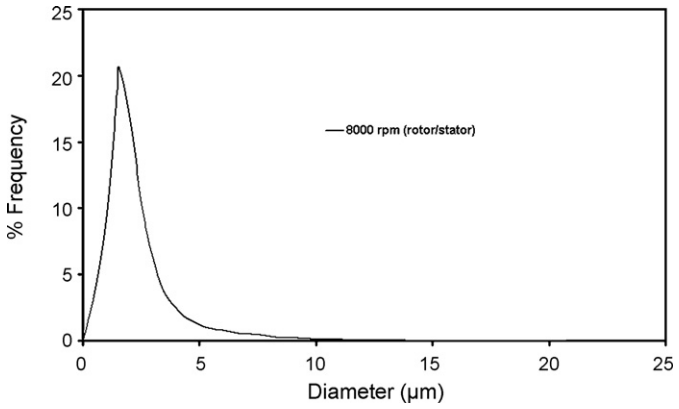

Fig. 4. Granulometric feature of the ARD microcapsules.

agitation is perceivable. Furthermore, some tiny solid particles deposed on the capsules surface can be observed. The formation of these particles can be attributed to precipitation of higher molecular weight melamine-formaldehyde pre-polymer in the continuous medium. An optical particle sizing instrument (Accusizer model 770 Particle Sizing systems) was used to characterize the number-average diameter of the microcapsules and the particle size distribution. The size distribution appears as quite homogenous and the particle diameter ranges from 2 to 4 μm (Fig. 4).

The nanoparticles from sample '18' have a mean diameter about 50 nanometers with relatively narrow size distribution as determined by SEM (Fig. 1). They seem to be aggregated with a nonspherical smooth shape.

The outer and inner surface morphologies of the microparticles 'E2' were observed with an optical microscope in the phase difference mode and with a Scanning Electron Microscope as shown in Fig. 5(top) and (bottom), respectively. The presence of nanoparticles '18' is shown in both images. The microparticles present an irregular and granular surface with a tougher and rougher outer shell due to the resin condensation takes place much faster in the boundary layer than in the continuous phase. The SEM micrograph (Fig. 5, bottom left) after breakage shows the inner surface of the microparticle. We can observe clearly the presence of small spheres resulting from the formation of an aggregated structure constituted of nanoparticles '18' linked together by the melamine-formaldehyde resin. In our previous work [15], we have shown that the particles have an occluded morphology and this rougher structure is mainly due to the spreading coefficients of the system. Thus, the nanoparticles tend to locate at the interface between the *n*-alkane and the amino resin. Therefore, they are either linked in the inner shell to form some sub-micromic particles or dispersed as nanoparticles in the core of the microparticles during the formation of the melamine-formaldehyde shell.

4.2. Latent heat

A conventional Different Scanning Calorimetry (DSC) was performed to prove that the polymer nanoparticles do not affect the latent heat. The thermal behavior of the microcapsules was recorded to analyse the influence of nanoparticles on latent heat

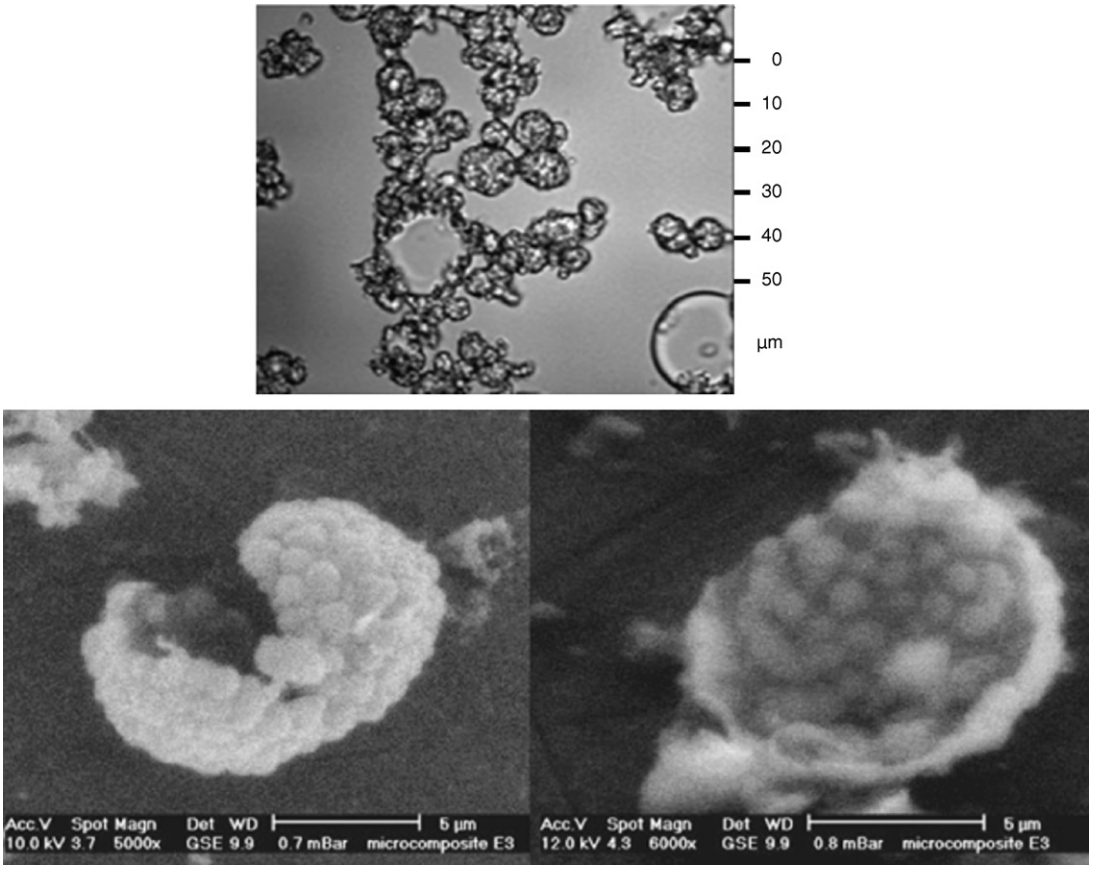

Fig. 5. Optical (top) and Scanning Electron Microscope (bottom) images of sample E2 proving the high density and the configuration of polymer nanoparticles inside the shell. Although shells include 68% of paraffin, the nanosized polymer particles generates a very dense and thermally insulating structure.

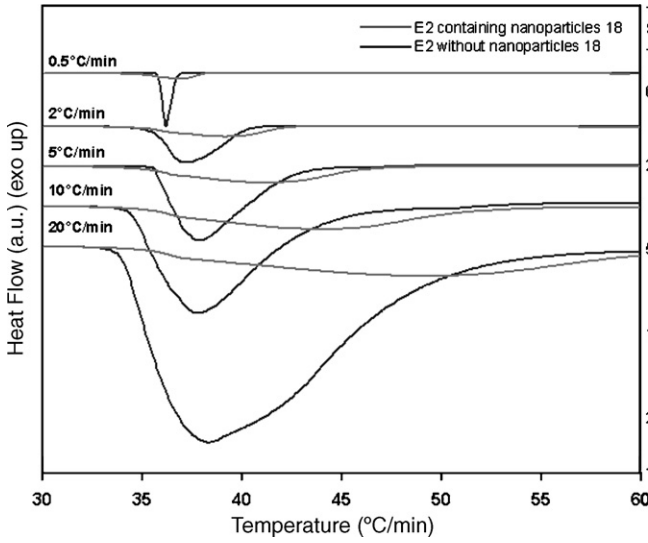

Scanning rate	Sample	T_{onset}	T_{max}	T_{offset}
0.5°C/min	E2 containing nanoparticles 18	34.81	36.84	38.10
	E2 without nanoparticles 18	35.67	36.14	36.53
2°C/min	E2 containing nanoparticles 18	35.00	39.14	42.14
	E2 without nanoparticles 18	35.58	37.20	40.33
5°C/min	E2 containing nanoparticles 18	34.95	41.14	46.88
	E2 without nanoparticles 18	35.55	37.78	42.12
10°C/min	E2 containing nanoparticles 18	35.06	43.96	52.04
	E2 without nanoparticles 18	34.41	37.80	43.99
20°C/min	E2 containing nanoparticles 18	34.78	49.12	63.05
	E2 without nanoparticles 18	33.99	38.35	50.02

Fig. 6. DSC characterization of the E2 sample showing the extension in the temperature interval of the phase change. Several increase rates for the temperature are displayed. Each of them leads to the same latent heat.

storage. The values of latent heat were found equal within the measurement accuracy for both *n*-eicosane encapsulated in a melamine-formaldehyde shell and polymer nanoparticles based microcapsules (sample 'E2'). The value of the latent heat is equal to 176 J/g. The DSC data reported in Fig. 6 however indicate a difference in the phase change behaviour. The temperature at which the solid-liquid transition starts is the same but the temperature span is 50% larger for the NPs based PCM compared to the conventional mirocapsules. The phase change will hence be effective on a larger temperature range. We presume that interaction between nanoparticle surface and paraffin induces a specific molecular structure in paraffin. This supposition is based on the analogy with the well-known layering of liquid molecules on a surface or around a particle [20]. This modification in the phase change is of course beneficial for textile application because temperature will be maintained under a broader heat flux amplitude.

4.3. Thermal conductivity

Fig. 7 reports on the thermal conductance G_{eq} against force for samples 18 and ARD. The slopes are not clearly different showing that the contact conductance is predominant over the sample conductance. But the difference in levels indicate that the paraffin in sample ARD is significantly more conductive than sample 18 including polymer. Eq. (1) provides the ratio of $\lambda_{18}/\lambda_{ARD} = 0.31$. From the reference data $\lambda_{ARD} = 0.26\ W\ m^{-1}\ K^{-1}$ and the very low thermal conductivity of $\lambda_{18} = 0.08\ W\ m^{-1}\ K^{-1}$ is found to be only three times the one of air.

Fig. 8 presents the evolution of the thermal conductance G_{eq} as a function of the electrical power in the probe. The hotter the probe is, the more resistive samples are. The linear behavior suggests that the samples might melt and become more resistive. The relative values of the samples thermal conductivities are reported in the inset of Fig. 8. Microparticle based samples, that are referred as E2 H/E and 18, are 60–70% more insulating than paraffin. This confirms the impact of the very insulating polymer nanoparticles on the PCM thermal conductivity.

Samples E2 and H/E include 68% of paraffin and 32% of polymer. Consequently, Maxwell-Garnett mixing rules predict a thermal conductivity decrease of 23%, which is about three-fold less the experimental data of 60%. The thermal resistances at interfaces between polymer nanoparticles and paraffin might explain such a discrepancy. A volume fraction of 10% also corresponds to an average inter-particle distance of 0.76 times the particle diameter, i.e. about 38 nm. We therefore suggest that percolating networks of

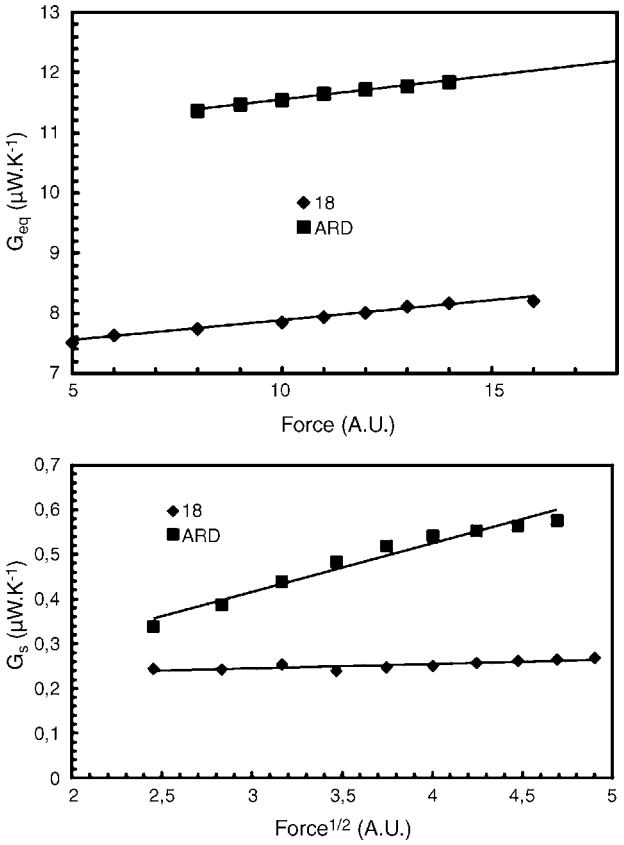

Fig. 7. (a and b) (top) Thermal conductance G_{eq} related to the heat flux exchanged between the thermal probe and the sample versus contact force between tip and sample. (bottom) Thermal conductance G_s of the sample versus contact force between tip and sample. The force is proportional to the tip deflection, which is measured by the photodiode presented in Fig. 5. The force units are hence provided by the photodiode signal in NanoAmperes.

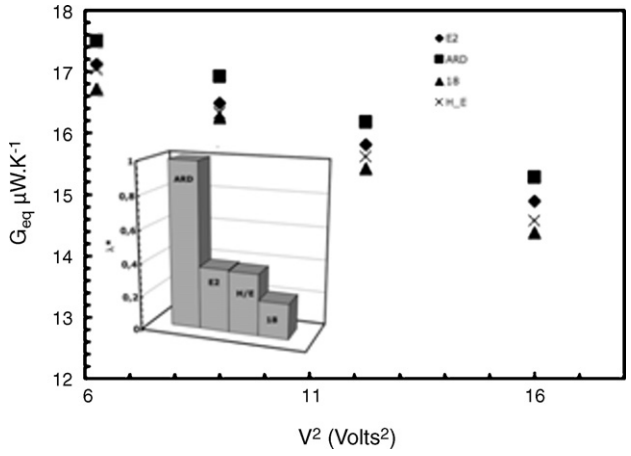

Fig. 8. Thermal conductance G_{eq} related to the heat flux exchanged between the thermal probe and the sample versus the input electrical tip voltage squared. The insert represents the normalized thermal conductivities of the four samples.

polymer nanoparticles might be responsible for the drastic reduction in heat conduction.

This property implies a considerable gain, especially in the field of textile because the temperature drop between the inner and the outer face is increased three-fold.

4.4. Bulk modulus

The Atomic Force Microscope allows for probing the mechanical properties of the surface. Fig. 9 provides the force applied on the tip versus the cantilever altitude. The stiffer the material is, the larger the slope is. Sample 18 is the stiffest material because it does not include any paraffin. The E2 sample has a lower melting point than H/E. The corresponding slope is the same as the one of sample 18 because we presume that the polymer contribution predominates because of its structural network included in a solid matrix. In sample H/E, paraffin is in the liquid phase at ambient which might explain the slight decrease of the slope. Isolated polymer nanoparticles might indeed slide among the aggregates. The ARD sample has the same slope as the H/E one in the range of the small forces because they include the same paraffin. The data point corresponding to the largest force seems to indicate that the capsule shell was broken. This mechanism appears only in the case of sample ARD because the polymer structure does not enforce the capsule.

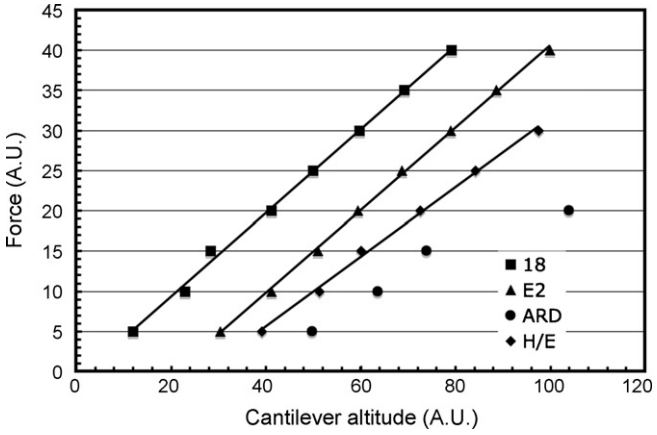

Fig. 9. Contact force between thermal probe and sample as a function of the tip height. The tip height is measured by the piezocrystal voltage.

5. Conclusion

We have synthesized core shell PCMs including polymer nanoparticles and have characterized their structural configuration via Scanning Electron Microscopy. The diameter of polymer nanoparticles is in the vicinity of 50 nm and the shell size is of a few microns. We have shown that the addition of polymer nanoparticles has a very beneficial impact on thermal properties. Both materials exhibited the same latent heat but the phase change occurs on a wider temperature interval in the case of the NP based PCM. Firstly, we have proven by using usual DSC that the temperature interval of the phase change is augmented by 50%. This significantly improves the role of thermal barrier of the PCM. We suppose that this effect is related to the ordered structure of paraffin molecules around the polymer nanoparticles. This configuration might require a larger amount of energy to start for melting.

Secondly; the value of the thermal conductivity of the polymer NPs was found to be extremely low, i.e. only twice the one of air. The addition of a reasonable fraction of NPs in the PCM capsule results in a decrease by a factor of three of the effective thermal conductivity. The outcome is a significant improvement of the thermal barrier in the steady state. The mechanical properties were estimated on a qualitative basis by using an atomic force microscope. The damage threshold was reached in the basic microcapsule before the one of the modified materials.

Appendix A

Eq. (1) is deduced from the expression of G_{eq}, which is the contact conductance G_c and the sample conductance G_S in series. The contact conductance is the result of the tip/sample conductances through air G_A and through the solid-solid contact G_{SS} in parallel. When the measurement is performed in ambient the slope of G_{eq} can be expressed as follows:

$$\frac{dG_{eq}}{dF} = \frac{d}{dF}\left[\frac{G_A + G_{SS} + G_S}{(G_A + G_{SS})G_S}\right] = \frac{1}{G_A G_S}\frac{dG_{SS}}{dF} \tag{A1}$$

because G_A and G_S are weakly dependent to the contact force and because previous works have shown that $G_{SS} \ll G_A$. G_S is proportional to the contact radius and to the sample thermal conductivity λ_S. G_{SS} is proportional to the contact radius squared. The contact radius can be defined in a general form as KF^a where F is the contact force and the power coefficient a and K are constants. According to Eq. (A1), the ratio between two slopes of G_{eq} measured on two different samples therefore yields:

$$\frac{\lambda_{S1}}{\lambda_{S2}} = \left(\frac{dG_{eq}/dF|_2}{dG_{eq}/dF|_1}\right)\left(\frac{K_2}{K_1}\right)^2 \tag{A2}$$

The same argument also applies to the force derivation of the sample conductance measured in vacuum:

$$\left(\frac{dG_S/dF|_2}{dG_S/dF|_1}\right) = \frac{K_2}{K_1}\frac{\lambda_{S2}}{\lambda_{S1}}, \tag{A3}$$

Combining Eqs. (A2) and (A3) leads to Eq. (1).

References

[1] Y.G. Bryant, D.P. Colvin, D.P., US Patent 4,756,958 (1988).
[2] K.E. Kaska, M.M. Chen, J. Sol. Energy Eng. 107 (1985) 229–236.
[3] J.C. Mulligan, D.P. Colvin, Y.G. Bryant, J. Spacecraft Rockets 33 (1996) 278–284.
[4] Y. Yamagishi, H. Takeuchi, A.T. Pyatenko, N. Kayukawa, AIChE J. 45 (1999) 696–707.
[5] N. Sarier, E. Onder, Thermochim. Acta 452 (2007) 149–160.
[6] V.V. Tyagi, D. Buddhi, Renew. Sustain. Energ. Rev. 11 (2007) 1146–1166.
[7] K. El Omari, J.P. Dumas, Int. J. Therm. Sci. 43 (2004) 1171–1180.
[8] M.N.A. Hawlader, M.S. Uddin, M.M. Khin, Appl. Energy 74 (2003) 195–202.

[9] H. Yoshizawa, E. Kamio, N. Hirabayashi, J. Jacobson, Y. Kitamura, J. Microencapsulation 21 (2004) 241–2349.
[10] M.L. Soto-Portas, J.F. Argillier, F. Méchin, N. Zydowicz, Polym. Int. 52 (2003) 522–527.
[11] M.S. Uddin, H.J. Zhu, M.N.A. Hawalder, Int. J. Solar Energy 22 (2002) 105–114.
[12] X. Zhang, X. Tao, K. Yick, X. Wang, Colloid Polym. Sci. 282 (2004) 330–336.
[13] J. Cho, Al. Kwon, C. Cho, Colloid Polym. Sci. 280 (2002) 260–266.
[14] Y.F. Fan, X.X. Zhang, X.C. Wang, J. Li, Q.B. Zhu, Thermochim. Acta 413 (2004) 1–6.
[15] F. Salaün, E. Devaux, S. Bourbigot, P. Rumeau, J. Appl. Polym. Sci. 107 (2008) 2444–2452.
[16] Q. Song, Y. Li, J. Xing, J.Y. Hu, Y. Marcus, Polymer 48 (2007) 3317–3323.
[17] S. Lefèvre, S. Volz, J.-B. Saulnier, C. Fuentes, N. Trannoy, Rev. Sci. Instrum. 74 (2003) 2418–2423.
[18] S. Lefèvre, S. Volz, Rev. Sci. Instrum. 76 (2005) 033701.
[19] S. Lefèvre, S. Volz, P.-O. Chapuis, Int. J. Heat Mass Transfer 49 (2006) 251–258.
[20] W. Yu, S.U.S. Choi, J. Nanoparticle Res. 5 (2004) 167–171.